ICWE14 June 21-26, 2015 | Porto Alegre - Brazil 14th INTERNATIONAL CONFERENCE ON WIND ENGINEERING

Analytical model for rocket effluent dispersion: sensitivity analysis

Bruno K. Bainy, Daniela Buske, Régis S. Quadros
Pos-Graduation Programme in Meteorology, Faculty of Meteorology, Universidade Federal de Pelotas, Pelotas, Brazil.
E-mail: bkbainy@hotmail.com, danielabuske@gmail.com, quadros99@gmail.com

ABSTRACT: This work shows some sensitivity analysis of a recently developed model for assess rocket effluent dispersion. The mathematical model for dispersion calculation is presented, as well as the turbulent parameterization used. Runs against experimental data (Hanford – 1983 and Copenhagen datasets) were carried in order to quantify the skill of the model, with good results. After that, a series of runs to test sensitivity of several important parameters is presented for both stable and unstable cases, for which the results are discussed. The study concluded that the model is able to represent properly dispersion in different conditions.

KEY WORDS: Pollution dispersion; Unsteady-state dispersion model; Short-term release; GILTT.

1 INTRODUCTION

The rocket exhaust transport is characterized by the turbulent diffusion phenomenon, which has not yet been stated in a unique and completely representative formulation, concerning all its internal processes [1]. The rocket launch process includes the immediate, previous and ahead instants to the launch. Within this time interval it occurs the combustion, in which a large hot and buoyant cloud is formed, and ascends until it reaches thermal equilibrium with the atmosphere. This referred cloud is called "ground-cloud", because it is generated near the ground level [2], and in normal launch conditions (excepting explosions and engine trials) it concerns a short-term release, from the order of 10 seconds [3]. The modelling of rocket exhaust generally concerns this cloud of pollutants. In the US, the model REEDM (*Rocket Exhaust Effluent Diffusion Model*) is traditionally used to this task. In Brazil, recently was developed a model called MSDEF (Modelo simulador de efluentes de foguetes, or *Model for Simulation of Rocket Effluenst* in a free translation), which is based on the mathematical procedure ADMM (advection diffusion multilayer model) to solve the advection-dispersion equation in a semi-analytic fashion, and also incorporating some of the north-american assumptions [1].

A similar approach to simulate rocket effluents has been proposed and developed using the Generalized Integral Transform Technique (GILTT) instead of the ADMM method. This paper aims to test the sensitivity some of some parameters that are of relevance to the considered problem.

2 METHODOLOGY

2.1 The mathematical model

The advection – diffusion equation was solved through GILTT in order to simulate finite releases. It contains terms of local storage of crosswind integrated concentration (c), mean wind advection, turbulent diffusion, gravitational settling (v_g), physical-chemical decay (λ) and precipitation scavenging (Λ_s), as shown in equation 1:

$$\frac{\partial c}{\partial t} + u\frac{\partial c}{\partial x} - v_g\frac{\partial c}{\partial z} = \frac{\partial}{\partial x}\left(K_x\frac{\partial c}{\partial x}\right) + \frac{\partial}{\partial z}\left(K_z\frac{\partial c}{\partial z}\right) - \lambda c - \Lambda_s c \quad (1)$$

The source is assumed to be of constant and short-termed release, as stated by equation 2:

$$c(0,z,t) = \frac{Q}{u}[\eta(t) - \eta(t - t_r)\delta(z - H_s)] \quad (2)$$

where δ is the Dirac delta function, η is the Heaviside step function and t_r is the duration of release.
The tri-dimensional concentration (c^*) profile is assumed to be Gaussian shaped, as in

$$c^*(x,y,z,t) = c(x,z,t) \cdot \frac{1}{\sqrt{2\pi}\,\sigma_y} e^{-\left[\frac{(y-y_0)^2}{2\sigma_y^2}\right]} \quad (3)$$

The initial condition provides zero concentration at t=0 and boundary conditions were assumed as zero contaminant flux at the top of the Planetary Boundary Layer (PBL) and non-zero flux at the ground level (there is deposition)

$$c(x,z,0) = 0 \quad (4)$$

$$K_z \frac{\partial c}{\partial z} = V_d c \qquad \text{at } z = z_0$$
$$K_z \frac{\partial c}{\partial z} = 0 \qquad \text{at } z = h, L_* \quad (5)$$

where V_d is the deposition velocity at the surface, z_0 is the roughness length, h is the PBL height and L_* is a distance far away from the source.

The solution via GILTT is based in some basic steps: the concentration is expanded in series based on the eigenfunctions attained to a Sturm-Liouville auxiliary problem; then, this expansion is replaced on the advection-diffusion equation. After that, the equation is integrated through all the planetary boundary layer height, generating a matrix ordinary differential equation, which is solved analytically using the Laplace transform, in order to solve the initial problem [4].
The first step is to apply the Laplace transform in eq. (1), resulting in

$$r\bar{c} - c(x,z,0) + u\frac{\partial \bar{c}}{\partial x} - v_g \frac{\partial \bar{c}}{\partial z} = \frac{\partial}{\partial x}\left(K_x \frac{\partial \bar{c}}{\partial x}\right) + \frac{\partial}{\partial z}\left(K_z \frac{\partial \bar{c}}{\partial z}\right) - \lambda\bar{c} - \Lambda_s\bar{c} \quad (6)$$

where $\bar{c}$ is the Laplace transform of concentration in the variable t ($\bar{c}(x,z,r) = \mathcal{L}\{c(x,z,t); t \to r\}$). The next step is to define the Sturm – Liouville auxiliary problem, and then expand the concentration in a sum. This auxiliary problem is chosen as function of the boundary conditions of the original problem. In this case it will be

$$\Psi_n''(z) + \lambda_n^2 \Psi_n(z) = 0 \qquad \text{for } z_0 < z < h, \quad (7)$$

with the same boundary conditions of the original problem, it is

$$\Psi_n'(z) = 0 \quad \text{for } z = h$$
$$K_z \Psi_n'(z) - V_d \Psi_n(z) = 0 \quad \text{for } z = z_0 . \quad (8)$$

The solution of the auxiliary problem serves as base to the expansion of the concentration in series and is given by

$$\Psi_n(z) = \cos\lambda_n(z - h), \quad (9)$$

in which the term λ_n refers to the eingenvalues of the auxiliary problem and satisfy the transcendental equation $\frac{V_d}{K_z(z_0)} = \lambda_n \tan[\lambda_n(h - z_0)]$, that is solved by the Newton – Raphson method. This way, it is possible to expand the concentration as

$$\bar{c}(x,z,r) = \sum_{n=0}^{\infty} \bar{c_n}(x,r)\Psi_n(z) . \quad (10)$$

The problem now consists in determining the values of $\bar{c_n}(x,r)$. Substituting this equivalence in eq. (6), taking moments (applying the operator $\int_0^h ()\Psi_m dz$, where Ψ_m is a function orthogonal to Ψ_n), truncating the sums to N terms, applying the derivation rules and rewriting the terms we obtain

$$\sum_{n=0}^{N} \frac{\partial c_n(x,r)}{\partial x} \int_0^h u(z)\Psi_n(z)\Psi_m(z)dz - v_g \sum_{n=0}^{N} c_n(x,r) \int_0^h \Psi_n'(z)\Psi_m(z)dz = \sum_{n=0}^{N} \frac{\partial^2 c_n(x,r)}{\partial x^2} \int_0^h K_x(z)\Psi_n(z)\Psi_m(z)dz + \sum_{n=0}^{N} c_n(x,r) \int_0^h K_z'(z)\Psi_n'(z)\Psi_m(z)dz + \sum_{n=0}^{N} c_n(x,r) \int_0^h K_z(z)\Psi_n''(z)\Psi_m(z)dz + (\lambda + \Lambda_s + r) \sum_{n=0}^{N} c_n(x,r) \int_0^h \Psi_n(z)\Psi_m(z)dz \quad (11)$$

This equation may be written in the matrix fashion, such as

$$Y''(x,r) + FY'(x,r) + GY(x,r) = 0, \quad (12)$$

in which the unknowns are vectors whose elements are $Y(x,r) = c_n(x,r)$, $Y'(x,r) = c_n'(x,r)$, $Y''(x,r) = c_n''(x,r)$, and $F = B^{-1}D$ and $G = B^{-1}E$ are matrixes constituted by

$$\begin{aligned} B &= \{b_{n,m}\} = \int_0^h K_x(z)\Psi_n(z)\Psi_m(z)dz, \\ D &= \{d_{n,m}\} = -\int_0^h u(z)\Psi_n(z)\Psi_m(z)dz, \quad \text{and} \\ E &= \{e_{n,m}\} = v_g \int_0^h \Psi_n'(z)\Psi_m(z)dz - \lambda_n^2 \int_0^h K_z(z)\Psi_n(z)\Psi_m(z)dz - (\lambda + \Lambda_s + r) \int_0^h \Psi_n(z)\Psi_m(z)dz + \int_0^h K_z'(z)\Psi_n'(z)\Psi_m(z)dz, \end{aligned} \quad (13)$$

reminding that $\Psi_n''(z) = -\lambda_n^2 \Psi_n(z)$.
Following the work [4], the next step is to reduce the order of Eq. 12, leading to

$$Z'(x,r) + H.Z(x,r) = 0 \quad (14)$$

where $Z(x,r) = col[Y(x,r), Y'(x,r)]$, and the matrix H has a block form $H = \begin{pmatrix} 0 & -I \\ G & F \end{pmatrix}$.
Applying the same procedures to the source condition (Eq. 2), we obtain

$$Y(0,r) = Q\left[\frac{1}{r} - \frac{e^{-r.t_r}}{r}\right] \frac{\Psi(H_s)}{u(H_s)} A^{-1} = Z(0,r) \quad (15)$$

in which A is a diagonal matrix given by $A = a_{n,m} = \int_0^h \Psi_n \Psi_m dz$.

Applying the Laplace transform in Eq. 14

$$s\bar{Z}(s,r) - Z(0,r) + H.\bar{Z}(s,r) = 0 \quad (16)$$

being $\bar{Z}(s,r)$ the Laplace transform of the vector $\bar{Z}(x,r)$. Assuming that the matrix H has distinct eigenvalues we may write $H = X.D.X^{-1}$, where D is the diagonal matrix of the eigenvalues and X is the respective matrix of eigenfunctions. Replacing this relation in eq. 16 and rearranging the terms leads to

$$(sI + X.D.X^{-1}).\bar{Z}(s,r) = Z(0,r) \quad (17)$$

where I is the identity matrix (since $X.X^{-1} = I$). In order to solve eq. 17 for Z(x,r) we must apply the inverse Laplace transform, as in

$$Z(x,r) = X.\mathcal{L}^{-1}\{(sI + D)^{-1}\}.X^{-1}.Z(0,r). \quad (18)$$

The term to which the inverse transform was applied is

$$\mathcal{L}^{-1}\{(sI+D)^{-1}\} = P(x,r) = \begin{pmatrix} e^{-d_1 x} & 0 & \dots & 0 \\ 0 & e^{-d_2 x} & \cdots & 0 \\ \vdots & \vdots & \ddots & \vdots \\ 0 & 0 & \cdots & e^{-d_N x} \end{pmatrix} \tag{19}$$

The solution is, then, given by

$$Z(x,r) = X.P(x,r).X^{-1}.Z(0,r) = M(x,r)\xi \tag{20}$$

in which $M(x,r) = X.P(x,r)$ and $\xi = X^{1}Z(0,r)$. Alternatively, we may rewrite eq. 20 as

$$\begin{pmatrix} Y(x,r) \\ Y'(x,r) \end{pmatrix} = \begin{pmatrix} M_{11}(x,r) & M_{12}(x,r) \\ M_{21}(x,r) & M_{22}(x,r) \end{pmatrix} \begin{pmatrix} \xi_1 \\ \xi_2 \end{pmatrix} \tag{21}$$

and to obtain the unknown vector ξ, we must solve the linear system

$$\begin{pmatrix} M_{11}(0,r) & M_{12}(0,r) \\ M_{21}(L_*,r) & M_{22}(L_*,r) \end{pmatrix} \begin{pmatrix} \xi_1 \\ \xi_2 \end{pmatrix} = \begin{pmatrix} Y(0,r) \\ Y'(L_*,r) \end{pmatrix}. \tag{22}$$

So far, the only numeric approximation concerns the truncation of the summation in eq. 10. In this work N was established as 90. The solution given in eq. 21 leads to Y(x, r), or $\bar{c_n}$(x, r). In order to obtain c(x,z,t) its necessary to multiply the solution by the inverse GILTT (eq. 10) and invert the Laplace transform in the time variable. This, here, was done through the Gaussian quadrature scheme, as

$$c(x,z,t) = \sum_{k=1}^{M} \frac{P_k}{t} A_k \sum_{n=0}^{N} \bar{c}_n \left(x, \frac{P_k}{t}\right) \Psi_n(z). \tag{23}$$

Where M is the order of the quadrature, A_k and P_k are respectively the weights and roots of the quadrature scheme tabulated [10]. More details on the solution and the inversion of the Laplace Transform procedure may be found in [4].

2.2 Experimental data for model validation

In order to validate the model, there were conducted simulations against experimental data. Due to lack of experiments of short – term emissions, the datasets from the experiments of Hanford – 83 and Copenhagen were used. This choice was based on the characteristics of the experiments: the first one concerns an emission from a low source, with tracer deposition, and within a stable Planetary Boundary Layer (PBL). The second one encompasses a high source emission in a convective PBL.

The Hanford experiment consists on six releases of the tracers ZnS (depositing) and SF_6 (non-depositing) from two different stacks, distant less than 1 m from the other and at 2 m height. Collectors were disposed over concentric circumferences at the distances of 100, 200, 800, 1600 and 3200 m from the source. The releases were made on stable to near-neutral PBL conditions, during a period of 30 minutes, except for the fifth run, which lasted for 22 minutes. The terrain roughness was 3 cm and the tabulated collected data (micrometeorological parameters and tracer) as well as further details of the experiments are found in [5].

The Copenhagen experiment was conducted under convective PBL conditions in a urban scenario, consisting on 9 releases of SF_6 without buoyancy from a stack 115 m high. Tracer was collected by samplers at ground level in arcs distant 2 to 6 km downwind from the source. The site roughness was 0.6 m. More information may be found in [6].

The statistical indexes used to quantify the model skills are

- Normalized Mean Square Error (NMSE): expresses the deviations between observed and calculated concentrations. Its ideal value is 1 and it is calculated as $NMSE = \frac{\overline{(C_o - C_p)^2}}{\overline{C_o}\,\overline{C_p}}$;

- Correlation Coefficient (COR): describes how well the variations of the observations are represented by the variations of the simulations. Its ideal value is 1 and it is given by $COR = \frac{\overline{(C_o - \overline{C_o})(C_p - \overline{C_p})}}{\sigma_o \sigma_p}$;
- Factor of 2 (FA2): Gives the percentage of data which satisfies $0.5 \leq \frac{C_p}{C_o} \leq 2$;
- Fractional Bias (FB): indicates if the model tends to overestimate or underestimate the values, based on the observations. Its optimum value is zero. If positive, indicates underestimation; if negative, overestimation. It is given by $FB = \frac{\overline{C_o} - \overline{C_p}}{0.5(\overline{C_o} + \overline{C_p})}$;
- Fractional Shift (FS): compares the observed and simulated standard – deviations. Its ideal value is zero, and it is defined as $FS = \frac{\sigma_o - \sigma_p}{0.5(\sigma_o + \sigma_p)}$.

2.3 Boundary layer parameterization and test cases

2.3.1 Stable case

The simulations were carried out using the Degrazia formulation for the turbulent diffusion in a stable PBL. The chosen vertical eddy diffusivity is given by [7]

$$K_z = \frac{0.3\left(1-\frac{z}{h}\right)u_* z}{1+3.7\left(\frac{z}{\Lambda}\right)} \tag{24}$$

in which $\Lambda = L(1 - z/h)^{5/4}$, h is the stable layer height and L is the Monin – Obukhov length.

The necessary data to run the model were mostly extracted from the experiment 2 of Hanford dataset. The source height was established to 10 m, mixing layer height of 135 m, $u_* = 0.26$ ms^{-1}, L = 44 m, u = 3.23 ms^{-1}(at 10 m height).

2.3.2 Unstable case

To an unstable PBL it is given by [8]

$$K_z = 0.22\,(w_* h)\left(\frac{z}{h}\right)^{1/3}\left(1-\frac{z}{h}\right)^{1/3}\left[1 - e^{-4z/h} - 0.0003e^{8z/h}\right] \tag{25}$$

The necessary data to run the model were mostly extracted from the experiment 1 of Copenhagen dataset. The source height was established to 10 m, mixing layer height of 1980 m, $w_* = 1.8$ ms^{-1}, L = -37 m, u = 2.1 ms^{-1} (at 10 m height).

For both stable and unstable cases, the duration of releases were defined in different values for short-term releases. All the concentrations are at ground level (1 m), and all the mentions of *concentration* refers to concentration under the centreline (line of maxima concentration), except when indicated another way. A brief summary of the test cases is given on Table 1. The mean wind vertical profile is given by the power law that is formulated as [9]

$$\frac{\bar{u}}{\overline{u_1}} = \left(\frac{z}{z_1}\right)^{\alpha} \tag{26}$$

for which $\bar{u}$ and $\overline{u_1}$ are the mean wind speed at the levels z and z_1, and α is a coefficient related to atmospheric turbulence, here established as 0.2.

Table 1: Summary information of test cases.

	Stable	Unstable
PBL height (m)	135	1980
L (m)	44	-37
u (10 m)	3.23	2.1
u_*/w_* (m.s^{-1})	0.26	1.8
Hs (m)	10	10
Q (kg.s^{-1})	100	100

3 RESULTS AND DISCUSSION

Statistical results on the comparisons against experimental data are shown in Table 2. Those values indicates good agreement with observation in both cases, meaning that the model was capable of representing very different stability and source conditions.

Table 2: Statistical indexes for the simulations.

	NMSE	COR	FA2	FB	FS
Hanford	0.18	0.820	1	-0.396	-0.431
Copenhagen	0.08	0.856	1	-0.013	0.013

Figure 1 shows the eddy diffusivities profile. It displays the behaviour of turbulent diffusion for the stability cases, the relative intensities and the regions of PBL where it has greater magnitudes. It is important to point out that the eddy diffusivity for the unstable situation reaches about one order of magnitude greater when compared to a stable PBL. Beyond that, it is necessary to consider that for an unstable PBL the region (height) of greater turbulent dispersion is in the middle boundary layer, while for a stable one it is in the lower layer. Figure 2 displays the simulated wind profiles for both cases. It is a must to notice that the ordinate axis is in a non-dimensional scale; even though the wind speed for the unstable case seems to be greater (and eventually becomes due to the power law for wind profile and the higher PBL), if we compares the speeds up to 130 m (PBL height for the stable case), the stable case has greater values (as it may also be seen on Table 1).

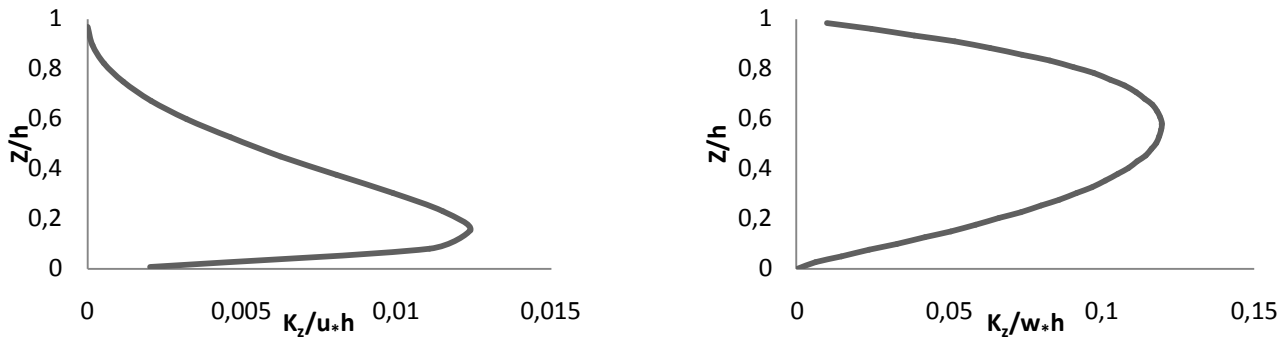

Figure 1: Non-dimensional eddy diffusivities profile for eq. 24 (stable case, left) and for eq. 25 (unstable case, right).

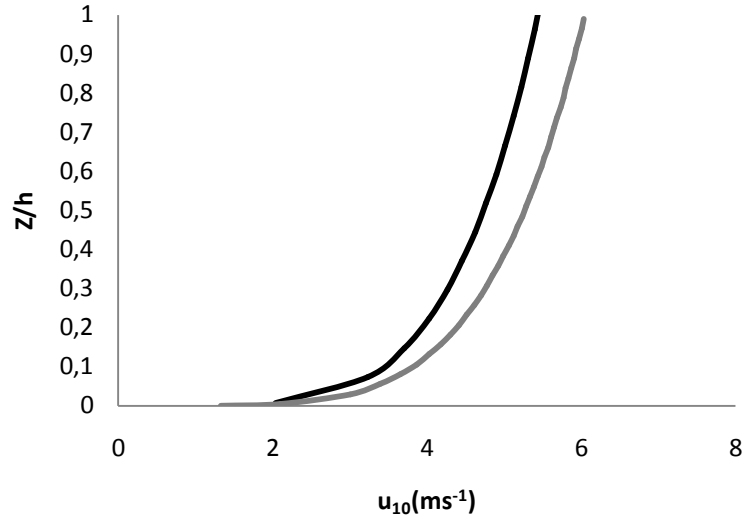

Figure 2: Wind profiles for the stable (black line) and unstable (gray line) cases.

The first sensitivity test is show in Figure 3, and shows the time evolution of concentrations predicted for both stable and unstable PBL considering different emission durations at 1000 m away from the source. Beyond the obvious fact that the greater the release time is, the greater concentrations it will produce, one may state that high concentrations tend to be more persistent in

a stable PBL than in an unstable one. For this case, though, it is necessary to remind that the difference between the established source height (10 m) and the height for which calculations were made (1 m) is relatively small. This fact, combined to the fact that eddy diffusivities on a stable PBL are much smaller than the ones in an unstable one indeed corroborates the maintenance of higher concentrations on the former case at heights similar to the emission heights, keeping the gradients longer. On the other hand, the turbulent diffusion (as explained by the gradient hypothesis) tends to increase concentrations where there is less pollution, diminishing the gradients.

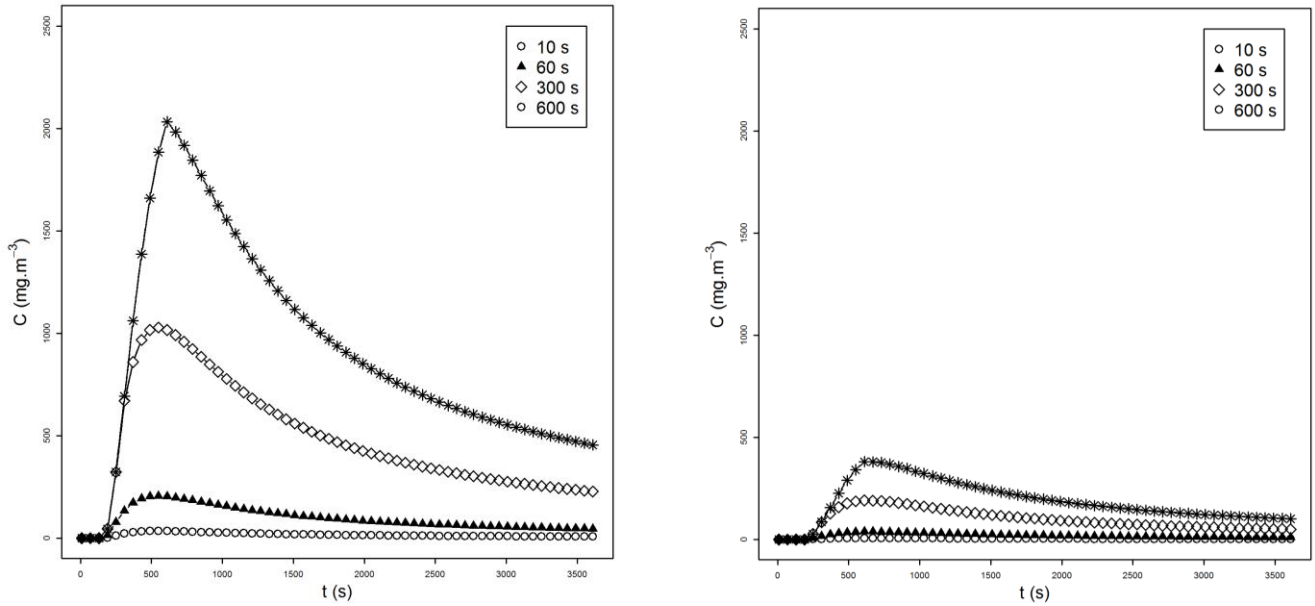

Figure 3: Time evolution of concentrations predicted at a point 1000 m far away from the source for the stable (left) and unstable (right) cases, in different durations of release.

For a steady state emission, it is possible to perceive similar trends. The huge difference in concentration between the cases exemplifies the efficiency of the turbulent diffusion for an unstable PBL. The ratios of the concentration for the stable case concerning the distances is about 44% for concentrations at 1000 m relative to 500 m and about 18% for concentrations at 2000 m. These ratios for the unstable case are about 38% and 18%, respectively.

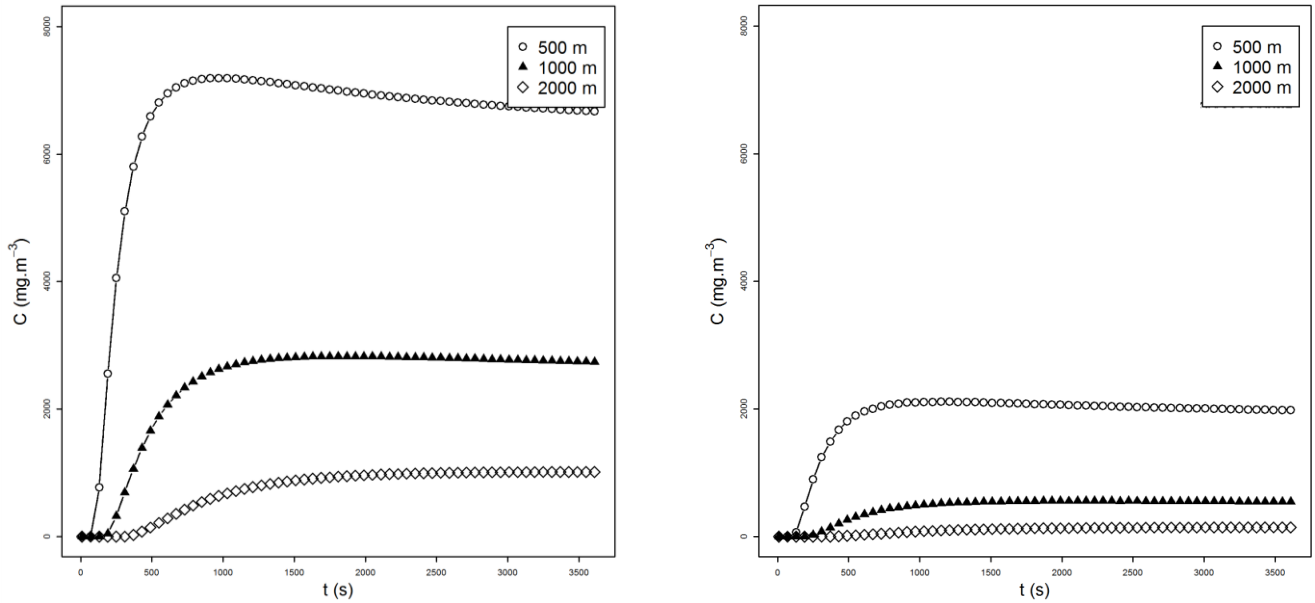

Figure 4: Time evolution of concentrations for the distances of 500, 1000 and 2000 m from the source for a steady state release ($t_r \geq t$), for the stable (left) and unstable (right) PBL cases.

The effect of source height may be better visualized with aid of Figures 5 (stable) and 6 (unstable). The concentration fields at 1 m height above ground level and t = 300 s for different relative heights (z/h) makes evident that the higher the source is, the further the maxima concentration will be from the source and the smaller those concentration will become, for both cases. For Figure 5 the relative heights of 0.1, 0.25, 0.5 and 0.75 correspond to 13.5, 33.75, 67.5 and 101.25 m respectively, while in Figure 6 those heights correspond to 198, 495, 990 and 1485 m respectively. Therefore, considering for both cases a stack of the same physical height we may state that: i) if the stack is a low source (*e. g.* 10 m, as in Figures 2 and 3), ground level concentrations will be greater in a stable PBL; and ii) if the stack is a higher source (such as 100 m) greater concentrations at the lower layer will be result of stronger turbulent dispersion in a unstable PBL. The pollutants reach the ground through the mechanisms of turbulent dispersion (dominant) and, in a much smaller scale, gravitational settling/deposition.

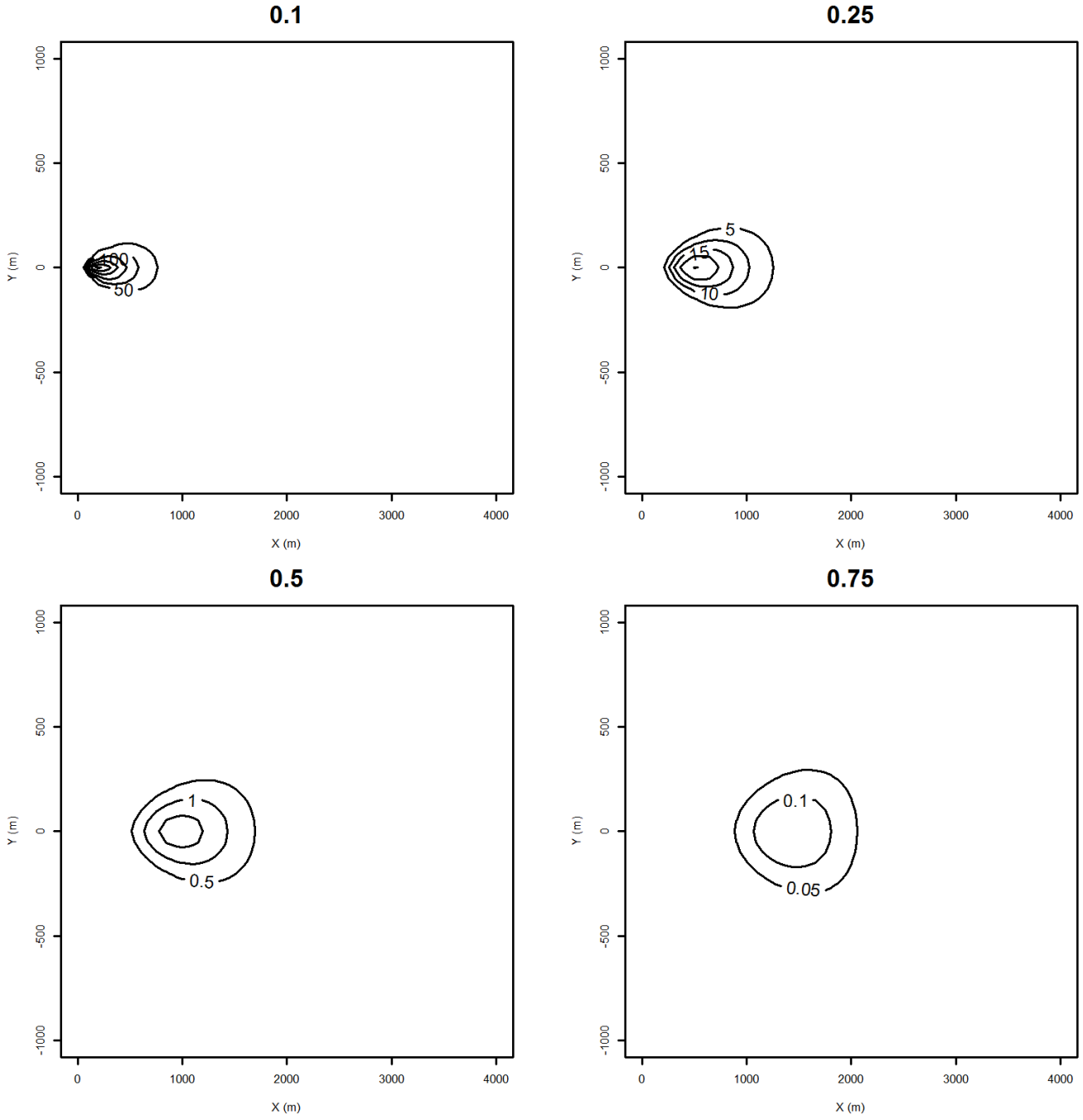

Figure 5: Ground level concentration isolines for t = 300 s after release at four different heights (H_s/h – 0.1, 0.25, 0.5, 0.75) for the stable case.

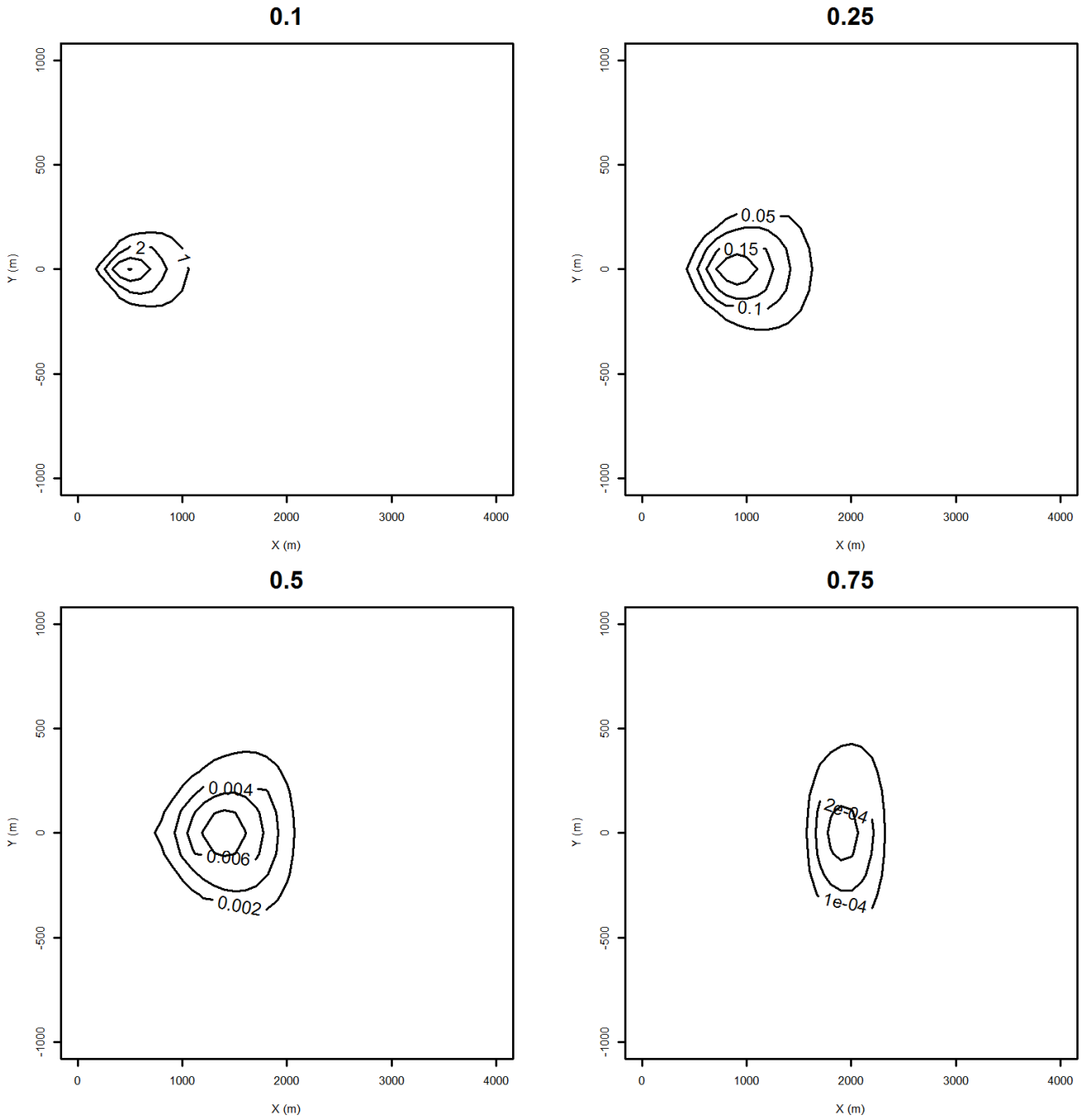

Figure 6: Ground level concentration isolines for t = 300 s after release at four different heights (H_s/h – 0.1, 0.25, 0.5, 0.75) for the unstable case.

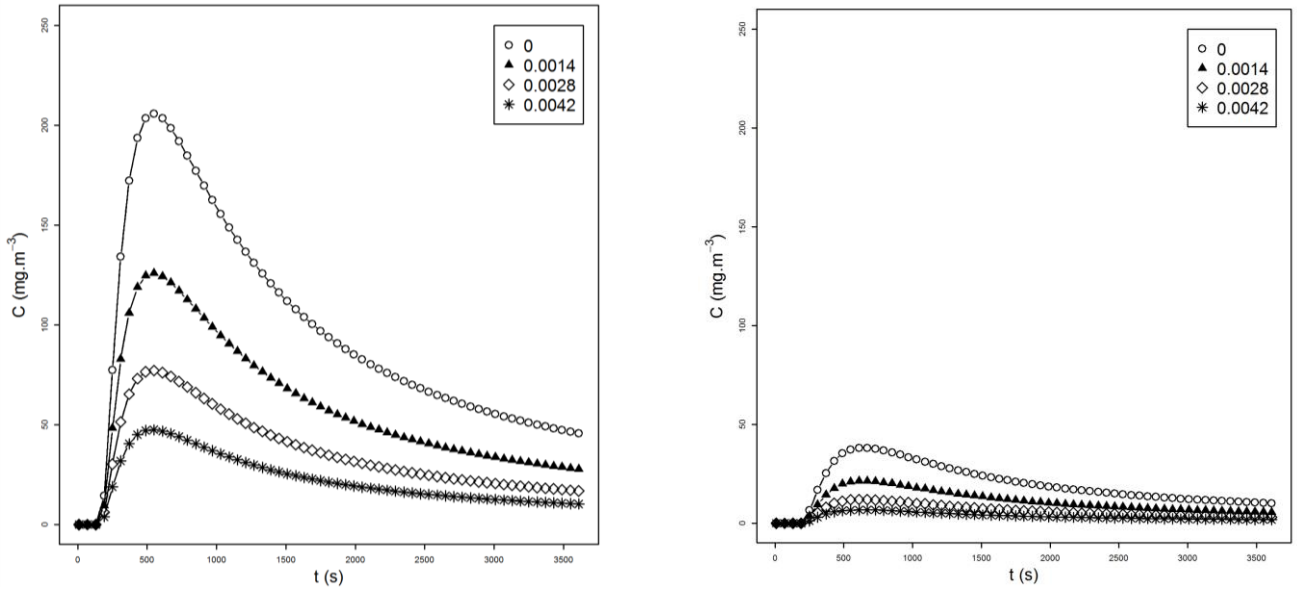

Figure 7: Centreline concentrations at 1000 m downwind away from the source for a duration release of 60 s and for different physical – chemical decay coefficients for the stable (left) and unstable (right) cases.

Figure 7 displays concentrations for the two cases and four different values for the physical – chemical decay coefficient [11]. The ratios of the concentrations regarding $\lambda = 0$ for the values of 0.0014, 0.0028 and 0.0042 are, respectively: 0.61; 0.37; 0.23 for the stable case and 0.56; 0.31; 0.17 for the unstable case.

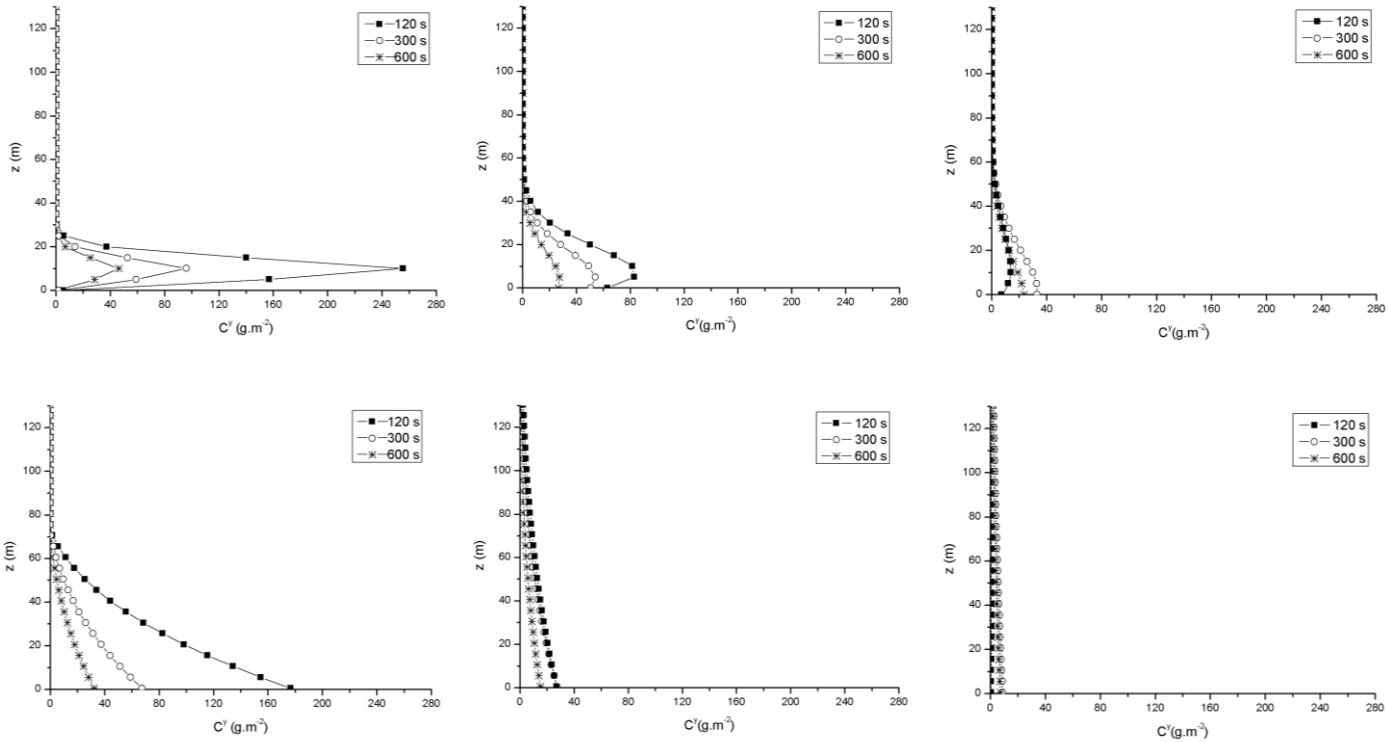

Figure 8: Vertical profile of pollutant crosswind integrated concentration for the stable (up) and unstable case (bottom), and t_r = 10 s for different time instants. Distances from source are 50 m (left), 250 m (centre) and 500 m (right).

Figure 8 illustrate the vertical profiles of crosswind integrated concentration for both cases, at the distances of 50, 250 and 500 m from the source and at different instants. It is very clear that contaminant gradients are maintained for the stable situation, preventing the cloud of pollution to spread wide on the vertical, while for unstable boundary layer it is noticeable the increased

vertical mixing, which seems to gain importance along the downwind direction. The difference of time instants at a same distance, however, seems to be due to wind advection mainly, instead of turbulent diffusion (the differences among the curves is horizontal, not vertical.).

4 CONCLUSIONS

The present study showed the sensitivity analysis for some considered parameters of a model which purpose is to simulate the rocket exhaust effluent diffusion. The model was proven statistically able to simulate properly on different stability and source conditions. Beyond that, the sensitivity tests were capable of not only showing the sensitiveness of several considered parameters, but also have proven consistency against the dispersion theory. Despite the inner complexity of the problem itself, advances are being made in order to improve the model structure and also possibly increase the knowledge concerning rocket launch air pollution problems.

AKNOWLEDGEMENTS

The authors thank FAPERGS (Fundação de Amparo à Pesquisa no Estado do Rio Grande do Sul) and project Pró-Estratégia (n. 2226/2012) for the partial financial support of this work.

REFERENCES

[1] Moreira, D. M; Trindade, L. B; Fisch, G.; Moraes, M. R; Dorado, R. M; Guedes, R. L.;.A multilayer model to simulate rocket exhaust clouds . **Journal of Aerospatial Technology and Management**, São José dos Campos, v. 3, n. 1, p. 41-52, 2011.

[2] Nyman, R.L.; NASA Report: Evaluation of Taurus II Static Test Firing and Normal Launch Rocket Plume Emissions. In:NASA.,**Final Report: environmental assessment for the expansion of the Wallops flight facility launch range**. NationalAeronauticsand Space Administration, 2009.Appendix G.

[3] Bjorklund, J.R.; Dumbauld, J.K, Cheney, C.S.; Geary, H.V.; **User's manual for the REEDM (Rocket Exhaust Effluent Diffusion Model) compute program**, NASA contractor report 3646. NASA George C. Marshall Space Flight Center, Huntsville, AL. 1982. 166p.

[4] Moreira, D. M.; Vilhena, M. T.; Buske, D.; Tirabassi,T. The state-of-art of the GILTT method to simulate pollutant dispersion in the atmosphere.**Atmospheric Research.**n. 92, p. 1-17, 2009.

[5] Doran, J. C.; Horst, T. W. An evaluation of Gaussian plume depletion modelswith dual-tracer field measurements. **Atmospheric Environment**, v.19, p.939–951, 1985.

[6] Gryning, S.; Holtslag, A.; Irwing, J.; Silversten, B. **Applied dispersion modeling based on scaling parameters**. Atmospheric Environment, v.21 (1), p.79–89, 1987.

[7] Degrazia, G. A.; Anfonssi, D.; Carvalho, J. C.; Mangia, C.; Tirabassi, T., Campos Velho, H. F. **Turbulence parametrisation for PBL dispersion models in all stability conditions**. Atmospheric Environment. v. 30, p.3575-3583, 2000..

[8] Degrazia, G. A., Rizza, U., Mangia, C., & Tirabassi, T. **Validation of a new turbulent parameterization for dispersion models in a convective boundary layer**. *Boudary Layer Meteorology* , 243-254, 1997.

[9] Panofsky, H. A.; Dutton, J. A. **Atmospheric Turbulence**. New York: John Wiley & Sons, 1984.

[10] Stroud, A., Secrest, D. (1966). **Gaussian quadrature formulas**. Englewood Cliffs, N.J.: Prentice Hall Inc.

[11] Bianconi, R., Tamponi, M. (1993). **A mathematical model of diffusion for a steady source of short duration in a finite mixing layer**. Atmospheric Environment , v.7, n.5, 781-792.